Journal of Quantitative Spectroscopy & Radiative Transfer 204 (2018) 250–255

Contents lists available at ScienceDirect

Journal of Quantitative Spectroscopy & Radiative Transfer

journal homepage: www.elsevier.com/locate/jqsrt

Small and large particle limits of single scattering albedo for homogeneous, spherical particles

H. Moosmüller[a,*], C.M. Sorensen[b]

[a] Laboratory for Aerosol Science, Spectroscopy, and Optics, Desert Research Institute, Nevada System of Higher Education, 2215 Raggio Parkway, Reno, NV 89512, USA

[b] Department of Physics, Kansas State University, 116 Cardwell Hall, 1228 N. 17th Street, Manhattan, KS 66506, USA

ARTICLE INFO

Article history:
Received 23 July 2017
Revised 28 September 2017
Accepted 28 September 2017
Available online 29 September 2017

Keywords:
Aerosol radiative forcing
Single scattering albedo
Rayleigh optics
Geometric optics
Complex refractive index
Mie theory

ABSTRACT

The aerosol single scattering albedo (SSA) is the dominant intensive particle parameter determining aerosols direct radiative forcing. For homogeneous spherical particles and a complex refractive index independent of wavelength, the SSA is solely dependent on size parameter (ratio of particle circumference and wavelength) and complex refractive index of the particle. Here, we explore this dependency for the small and large particle limits with size parameters much smaller and much larger than one.

We show that in the small particle limit of Rayleigh scattering, a novel, generalized size parameter can be introduced that unifies the SSA dependence on particle size parameter independent of complex refractive index. In the large particle limit, SSA decreases with increasing product of imaginary part of the refractive index and size parameter, another generalized parameter, until this product becomes about one, then stays fairly constant until the imaginary part of the refractive index becomes comparable with the real part minus one. Beyond this point, particles start to acquire metallic character and SSA quickly increases with the imaginary part of the refractive index and approaches one.

1. Introduction

The aerosol single scattering albedo (SSA) is the dominant intensive particle parameter determining aerosol direct radiative forcing. Chýlek and Wong [6] have given a simple analytical equation that estimates aerosol radiative forcing as function of SSA and the aerosol upscatter fraction. This equation becomes very useful when the aerosol upscatter fraction is properly related to the aerosol backscatter fraction or the asymmetry parameter [17]. Recently, the aerosol radiative forcing equation of Chýlek and Wong [6] has been compared with the output of a global Monte-Carlo Aerosol Cloud Radiation (MACR) model and been found adequate for cloud-free conditions [8].

For homogeneous, spherical particles, the SSA can easily be obtained from Mie theory [13] calculations as function of the particle complex refractive index m with

$$m = n + i\,\kappa, \tag{1}$$

where n and κ are the real and imaginary parts of the refractive index, respectively, and the size parameter x with

$$x = \frac{\pi D}{\lambda}, \tag{2}$$

where D is the particle diameter and λ the wavelength of the incident light. Note that the bulk or material absorption coefficient $\alpha = 4\pi\kappa/\lambda$ is directly related to the imaginary parts of the refractive index. For a complex refractive index independent of wavelength, the SSA is solely dependent on size parameter x and complex refractive index m. We build upon the initial discussions of aerosol SSA size dependence by Moosmüller and Arnott [15], Moosmüller et al. [16], and Sorensen [19]. In Fig. 1, we show a log-log plot of single scattering albedo (*SSA*) calculated with Mie (solid lines) and Rayleigh (dashed narrow lines) theory as function of size parameter x for several different values of the imaginary part κ of the particle refractive index and a typical real part (i.e., $n = 1.5$). In this figure, three different regimes can be distinguished and are approximately separated by vertical dashed lines: (1) The Rayleigh regime where $x << 1$ and consequently the incident light wave uniformly penetrates the particle and light scattered by the different sub-volumes of the particle is in phase, with amplitudes coherently adding. This leads to scattering and absorption cross-sections proportional to particle volume squared and volume,

* Corresponding author.
E-mail addresses: Hans.Moosmuller@dri.edu (H. Moosmüller), sor@phys.ksu.edu (C.M. Sorensen).

https://doi.org/10.1016/j.jqsrt.2017.09.029

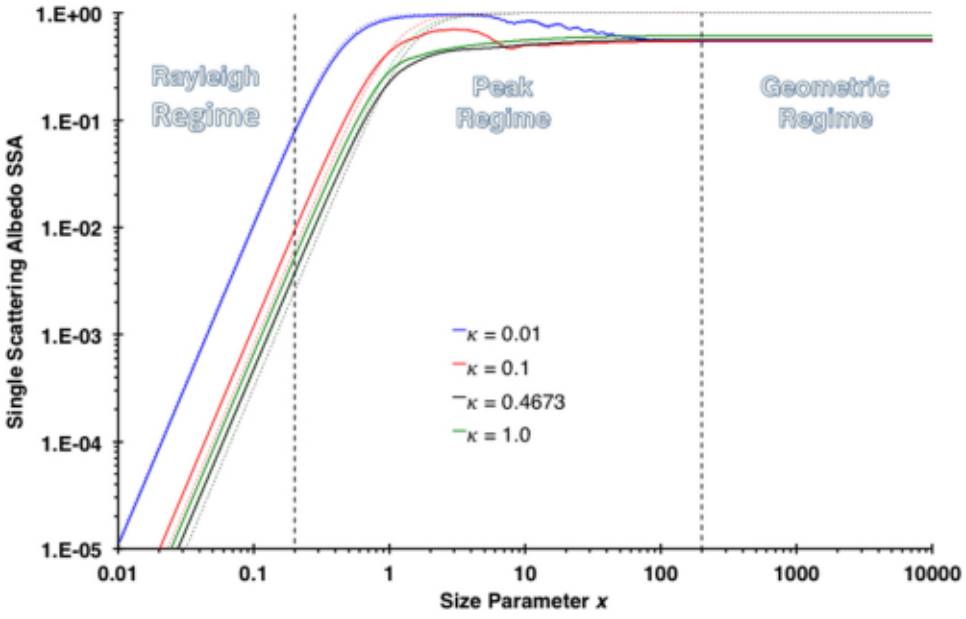

Fig. 1. Single scattering albedo *SSA* as function of size parameter x for a refractive index $m = 1.5 + i\,\kappa$ with Mie and Rayleigh calculations shown as solid and dashed lines, respectively. Vertical dashed lines indicate approximate boundaries between Rayleigh, peak, and geometric regimes. (For interpretation of the references to color in this figure legend, the reader is referred to the web version of this article.)

respectively, and to an SSA quickly increasing with size parameter x; (2) The "peak" regime, where for small imaginary parts of the refractive index (i.e., $\kappa << 1$), the SSA peaks and shows ripples; and (3) the geometric optics regime of our everyday visual experience, where the SSA is independent of size parameter x. In the following, we will discuss the small and large particle limits of SSA in the context of Fig. 1.

2. Small particle limit

In the small particle limit ($x << 1$) we can use Rayleigh theory for a simpler and more understandable description of particle scattering and absorption than given by Mie theory [4]. Rayleigh theory uses the Lorentz-Lorenz factor $LL(m)$ [11,12] given by

$$LL(m) = \frac{m^2 - 1}{m^2 + 2}, \tag{3a}$$

with $E(m)$ and $F(m)$ conventionally used to denote imaginary part and complex square of LL, respectively [19] as

$$E(m) = Im\{LL(m)\} \text{ and } F(m) = |LL(m)|^2. \tag{3b}$$

In the Rayleigh regime ($x << 1$), Rayleigh particle scattering efficiency Q_{sca_Ray} and absorption efficiency Q_{abs_Ray} (both ratios of optical to geometric cross-section) can be written simply as

$$Q_{sca\_Ray}(x, m) = \frac{8}{3} x^4 F(m) \text{ and} \tag{4a}$$

$$Q_{abs\_Ray}(x, m) = 4x E(m). \tag{4b}$$

The SSA, the ratio of scattering and extinction cross-sections (where the extinction cross-section is the sum of scattering and absorption cross-sections) can be written in terms of efficiencies as

$$SSA(x, m) = \frac{Q_{sca}}{Q_{ext}} = \frac{Q_{sca}}{Q_{sca} + Q_{abs}} = \left[1 + \frac{Q_{abs}}{Q_{sca}}\right]^{-1}, \tag{5a}$$

where Q_{ext} is the extinction efficiency. Using the explicit expressions for Q_{sca_Ray} and Q_{abs_Ray} given in Eq. (4) yields SSA_{Ray}, the SSA in the Rayleigh regime as

$$SSA_{Ray}(x, m) = \left[1 + \frac{1.5}{\left(\frac{F(m)}{E(m)}\right) x^3}\right]^{-1}. \tag{5b}$$

Defining a function f of the complex refractive m as the ratio of $F(m)$ and $E(m)$

$$f(m) = \frac{F(m)}{E(m)} \tag{5c}$$

allows one to write

$$SSA_{Ray}(x, m) = \left[1 + \frac{1.5}{f(m)\, x^3}\right]^{-1}, \tag{5d}$$

where the dependence of SSA_{Ray} on size parameter x and refractive index m is cleanly separated. This expression can be expanded into a power series with respect to size parameter x as

$$SSA_{Ray}(x, m) = \frac{2}{3} f(m) x^3 - \frac{4}{9} f(m)^2 x^6 + \frac{8}{27} f(m)^3 x^9 - \ldots, \tag{5e}$$

where for $x << 1$, SSA_{Ray} is proportional to x^3 and to $f(m)$. With increasing x, higher order terms come into play and SSA_{Ray} converges monotonically to one (Fig. 1). However, as x increases, we leave the Rayleigh regime and Eq. (5) are no longer valid; the Rayleigh solution diverges from the Mie result (Fig. 1).

Within the Rayleigh regime, the refractive index function $f(m)$ determines the dependence of the SSA_{Ray} on the refractive index m. For a common real part of the refractive index, that is $n = 1.5$, $f(m)$ and therefore SSA_{Ray} have one minimum (i.e., local and global; see Fig. 2) for $\kappa_{min}(n = 1.5) = 0.4673$ with

$$f_{min}(1.5 + i\,\kappa) = f(1.5 + i\,0.4673) = 0.7204 \text{ and consequently} \tag{6a}$$

$$SSA_{Ray\_min}(1.5 + i\,\kappa) = SSA_{Ray}(1.5 + i\,0.4673) = \left[1 + \frac{1.5}{0.7204 x^3}\right]^{-1}. \tag{6b}$$

A plot of this minimum SSA_{Ray} as function of x for $\kappa = 0.4673$ is included in Fig. 1.

Obviously, the imaginary part of the refractive index yielding minimum $f(m)$ for any size parameter in the Rayleigh regime is a function of the real part n of the refractive index. Fig. 3 shows a contour plot of the refractive index function $f(m)$ as function of

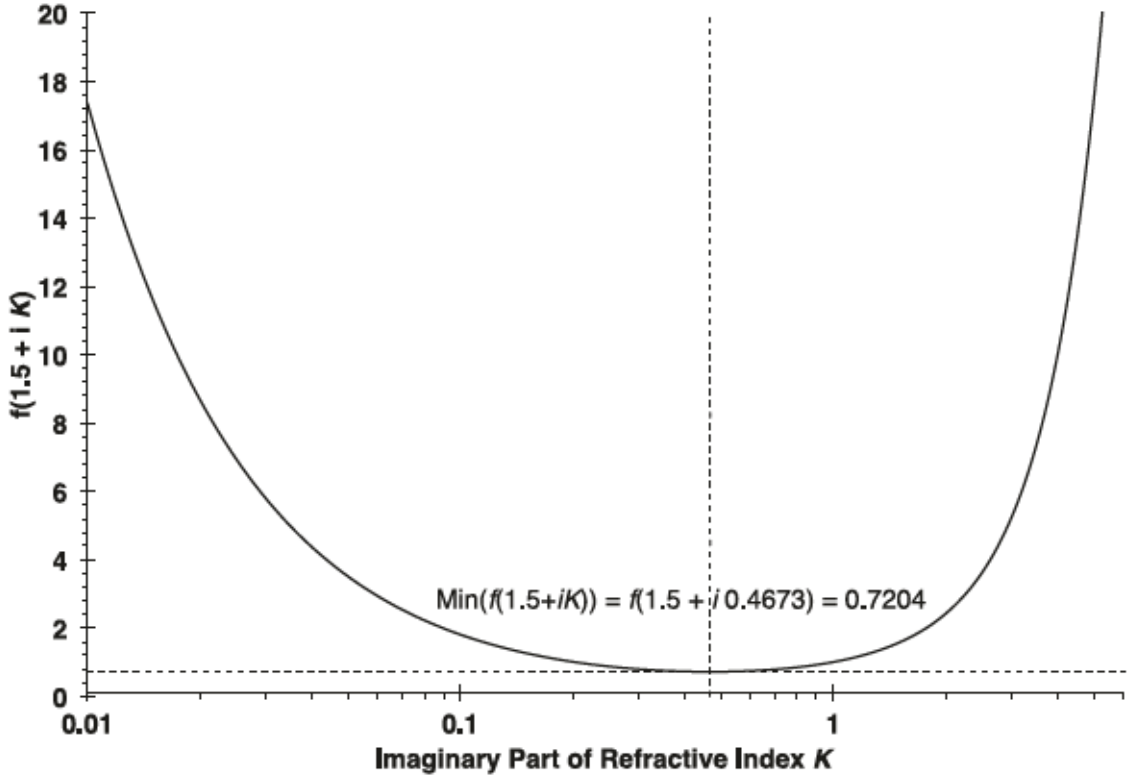

Fig. 2. Refractive index function $f(m)$ for $m = (1.5 + i\,\kappa)$ as function of κ. The minimum of $f(m) = 0.7204$ is marked with thin dashed lines.

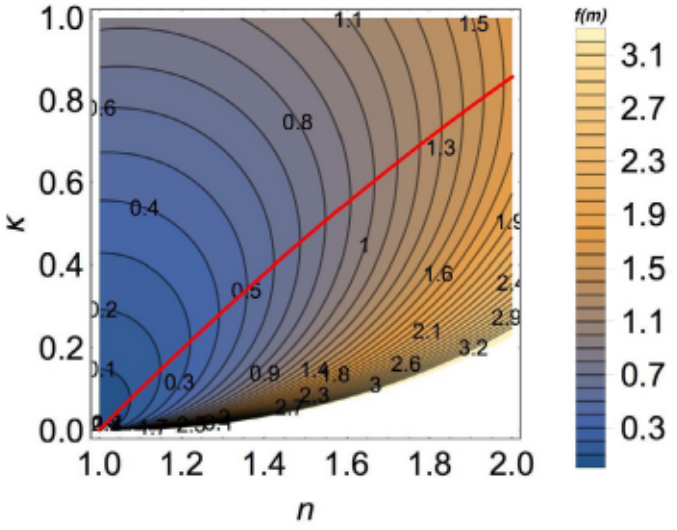

Fig. 3. Contour plot of the refractive index function $f(m)$ as function of the real part n (x-axis) and the imaginary part κ of the complex refractive index m. The values of $f(m)$ are indicated by labeled contours and by a color scale shown on the right. The red line shows $\kappa_{min}(n)$, that is, the imaginary part of the refractive index as function of the real part of the refractive index at which the minimum of $f(m)$ occurs. Note that this is where the slopes of the contours are infinite so that as one moves vertically with κ (at constant n), a minimum in $f(m)$ occurs. (For interpretation of the references to color in this figure legend, the reader is referred to the web version of this article.)

the real part n (x-axis) and the imaginary part κ (y-axis) of the complex refractive index m. The minimum of SSA_{Ray} for a given size parameter x occurs at an imaginary part of the refractive index $\kappa_{min}(n)$, which in Fig. 3 is indicated as red line. Note that this line crosses SSA contour lines at their maximum n. A simple analytical approximation of the function $\kappa_{min}(n)$ is useful to estimate at what combination of real and imaginary parts of the refractive index SSA_{Ray} is minimized; it is given for $1 < n < 2$ by a quadratic function as

$$\kappa_{min}(n) = -1.159 + 1.312\ \mathrm{n} - 0.1517\ n^2. \tag{7}$$

An alternative view considers SSA_{Ray} as a function of a novel, generalized Rayleigh size parameter (which we define here) $\xi_{Ray}(x,m)$ with

$$\xi_{Ray} = \sqrt[3]{\frac{2}{3} f(m)}\, x\ , \tag{8a}$$

yielding SSA_{Ray} only depending on this generalized size parameter as

$$SSA_{Ray}(x,m) = \left[1 + \xi_{Ray}{}^{-3}\right]^{-1} \approx \xi_{Ray}^3, \tag{8b}$$

with a single unified SSA curve within the Rayleigh regime [see also Eq. (114) in [19]]. In Fig. 4, this is demonstrated by plotting the Mie calculations from Fig. 1 not as a function of size parameter x but as function of the generalized Rayleigh size parameter $\xi_{Ray}(x,m)$, resulting in a single curve SSA_{Ray} (i.e., for $x << 1$) for all refractive indices shown, as obvious from Eq. (8). Note that this generalized Rayleigh size parameter is distinctly different from the internal coupling parameter ρ', previously proposed to describe scattering (but not absorption) from absorbing spheres [9].

3. Large particle limit

In the large particle limit ($x >> 1$), we can use geometric optics plus diffraction theory for a simpler and more understandable description of particle scattering and absorption than given by Mie theory. Fig. 1 indicates that for $x >> 1$, the SSA is independent of size parameter x, having converged toward the geometric limit $SSA_{geo}(m)$, which is exclusively a function of the complex refractive index m. $SSA_{geo}(m)$ is the ratio of the scattering efficiency

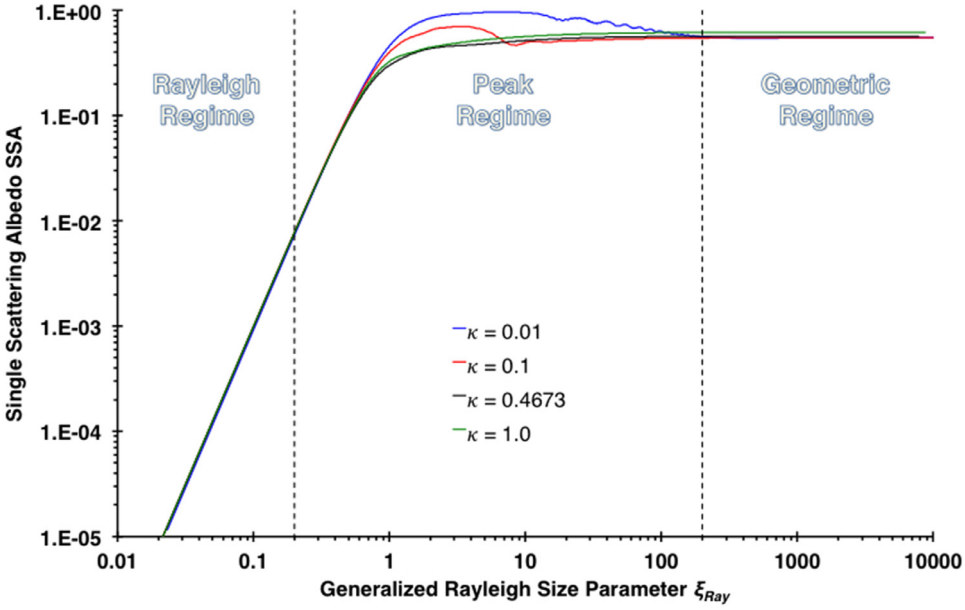

Fig. 4. Mie calculations of the single scattering albedo *SSA* (Fig. 1) as function of the novel, generalized Rayleigh size parameter $\xi_{Ray}(x,m)$ for a refractive index $m=(1.5+i\,\kappa)$. Note that within the Rayleigh regime ($\xi_{Ray}<<1$), SSA_{Ray} depends exclusively on the generalized Rayleigh size parameter ξ_{Ray}. Vertical dashed lines indicate approximate boundaries between Rayleigh, peak, and geometric regimes. (For interpretation of the references to color in this figure legend, the reader is referred to the web version of this article.)

$Q_{sca\_geo}(m)$ and the extinction efficiency Q_{ext_geo} (m) in the geometric regime ($x>>1$). It is generally accepted that $Q_{ext\_geo}=2$, independent of the complex refractive index m [e.g., [4]]; this is known as extinction paradox and commonly explained by geometric optics plus diffraction [20]; however, other viable explanations have been recently put forward [2]. The large particle limit Q_{sca_geo} of the scattering efficiency Q_{sca} has been the subject of some discussion in the sixties and seventies [1,3,5,7,10]. Bohren and Huffman [4] have summarized this discussion concluding that the scattering efficiency $Q_{sca\_geo}(m)=Q_{diff}+Q_{refl}(m)=1+Q_{refl}(m)$, where the diffraction efficiency $Q_{diff}=1$ and Q_{refl}(m) is the geometric optics external reflection efficiency. Note that this approximation, used by [3] and by us, ignores transmission and internal reflections which is appropriate for large, sufficiently absorbing spheres because all light entering the sphere is absorbed before reemerging. An explicit example is a sphere with infinite diameter and size parameter and any non-zero imaginary part of the refractive index [4].

Let us first revisit Fig. 1 of Bohren and Herman ([3]; reproduced as Fig. 7.4 in Bohren and Huffman [4]), the data of which are shown with some additions in our Fig. 5. This figure shows, for a complex refractive index $m=1.3+i\ 0.1$, the scattering efficiency Q_{sca} as function of the inverse size parameter x^{-1}, thereby simplifying the visualization of $x\to\infty$ or $x^{-1}\to 0$. The original results by Bohren and Herman [3] obtained with Mie code and geometric optics plus diffraction are shown as crosses and dashed line, respectively; our calculations (labeled "M & S") are added as solid lines for both cases, and the 0° Fresnel reflection plus diffraction result by Herman [10] as dotted line. Geometric optics plus diffraction and 0° Fresnel reflection plus diffraction results are independent of size parameter. For geometric optics plus diffraction, Bohren and Herman [3] give $Q_{sca\_geo}(1.3+i\ 0.1)=1.0647$; however, the same figure, reprinted as Fig. 7.4 in Bohren and Huffman [4] gives $Q_{sca\_geo}(1.3+i\ 0.1)=1.067$ in the figure caption, this is likely a typographical mistake that is in clear disagreement with the figure itself. Our geometric optics plus diffraction calculations are based on the equations summarized by Moosmüller and Arnott [14] and yield a slightly (~0.2%) larger value of $Q_{sca\_geo}(1.3+i\ 0.1)=1.06488$, probably due to differences in the numerical integration. For Mie calculations, again the $Q_{sca\_Mie}(x,\ m=1.3+i\ 0.1)$ values of Bohren and Herman [3], digitized from their Fig. 1, are in good agreement with our (M & S) Mie calculations as shown in Fig. 5. However, we have extended our Mie calculations by three orders of magnitude beyond their maximum size parameter of $x_{max}\sim 10^4$ to $x_{max}=10^7$, which (in Fig. 5) shows much more clearly the convergence of Mie and geometric optics plus diffraction calculations for the $x\to\infty$ or $x^{-1}\to 0$ limit with $Q_{sca\_Mie}(x=10^7,\ m=1.3+i\ 0.1)=1.06492$ within 0.004% of our geometric optics plus diffraction result. Either set of calculations clearly shows the discrepancy with the results of the early "flat sphere" approximation by Herman [10].

Next, we explore $SSA_{geo}(m)$ as function of m, that is as a function of real and imaginary refractive indices n and κ, respectively. In Fig. 1 it can be seen that for $x=10^4$ and $n=1.5$, *SSA* increases with increasing imaginary part κ of the refractive index for κ between 0.01 and 1.0. This is explored in more detail in Fig. 6 where $SSA_{geo}(m)$ is calculated from Mie theory for a very large sphere (geometric limit, size parameter $x=10^7$) and plotted as function of imaginary part κ of the refractive index (upper x-axis) and as function of κx (lower x-axis), the ratio of particle radius and skin depth [18,21]. Note that for very small (10^{-3}) κx, $SSA\cong 1$; as κx increases, *SSA* rapidly decreases, reaching a near constant value at $\kappa x\approx 1$. The geometric optics plus diffraction interpretation is that diffraction, external reflection, and transmission including internal reflection all contribute to particle scattering for $\kappa x<<1$. As κx grows toward one (indicated in Fig. 6 by a vertical, dashed line) the transmission is virtually eliminated because the skin depth is now comparable to the particle radius and scattering is due to diffraction with scattering efficiency of $Q_{diff}=1$ and Fresnel reflection with scattering efficiency of $Q_{refl}(m)$, while all the light entering the particle is absorbed with $Q_{abs}(m)=2-(Q_{refl}(m)+Q_{diff})$. For real parts of the refractive index $1<n<2$ this leads to $0.5<SSA<0.6$. The higher n, the higher SSA in this region due to increased Fresnel reflection. However, above $\kappa x\approx 1$, SSA becomes fairly independent of the imaginary part of the refractive index κ because the skin depth is very thin compared to the radius and hence effective regardless of its depth. However, once κ becomes comparable to $n-1$ (indicated in Fig. 6 by a vertical, dashed line for $\kappa=0.5$, as

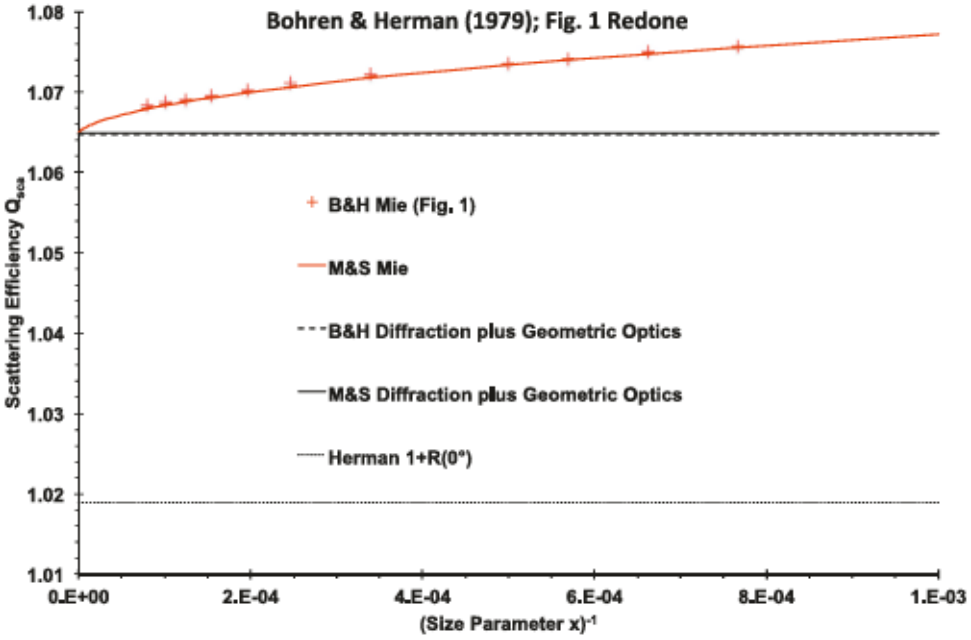

Fig. 5. A re-plot of results shown in Bohren and Herman ([3]; Fig. 1) for a complex refractive index $m = 1.3 + i\ 0.1$, with our (M&S) Mie and "Diffraction plus Geometric Optics" calculations added as solid lines. The large size parameter limit of our Mie calculations ($x = 10^7$) corresponds to $x^{-1} = 10^{-7}$, which, in this plot looks nearly identical to $x = 0$, clearly showing the convergence of Mie and geometric optics calculations.(For interpretation of the references to color in this figure legend, the reader is referred to the web version of this article.)

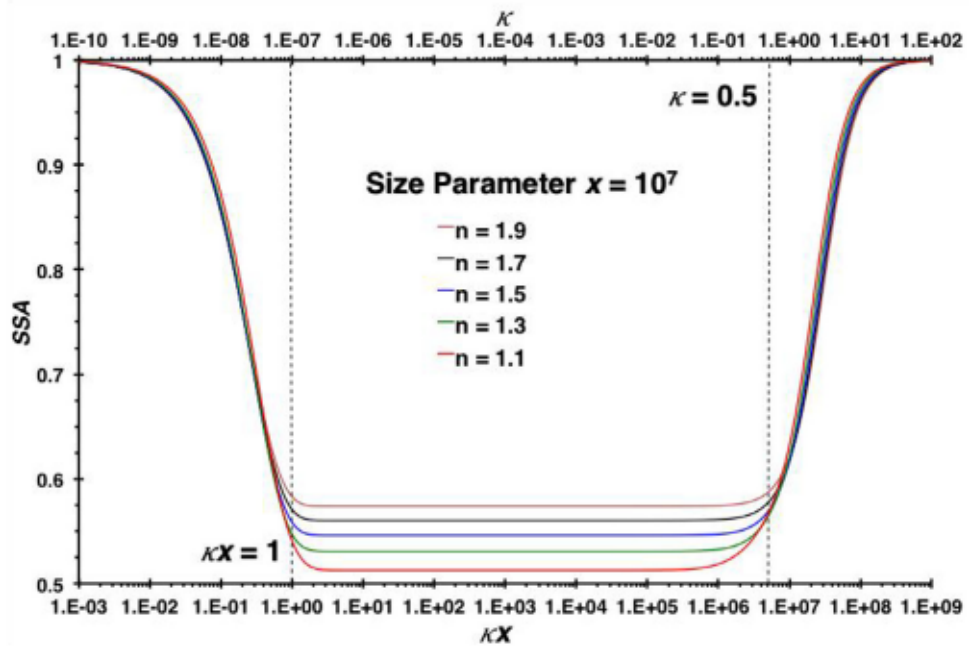

Fig. 6. Single scattering albedo (SSA) calculated with Mie theory for a very large ($x = 10^7$) sphere as function of κx, the ratio of particle radius and skin depth. Note that vertical dashed lines indicate $\kappa x = 1$, above which SSA becomes nearly constant because most light transmitted through the particle is absorbed and $\kappa = 0.5$, above which particles acquire a metallic character and SSA increases toward one. (For interpretation of the references to color in this figure legend, the reader is referred to the web version of this article.)

appropriate for $n = 1.5$), particles start to acquire metallic character with greatly increased Fresnel reflection and SSA quickly increases with κ, and approaches one (Fig. 6). In summary, Fig. 6 shows how the imaginary part of the refractive index κ first causes absorption to decrease the SSA, the absorption saturates when $\kappa x \gtrsim 1$, but ultimately large κ combines with the real part n to cause significant metallic reflection which causes the SSA to increase again and to approach one.

4. Conclusions

In conclusion, we have shown that in the small particle limit of Rayleigh scattering ($x << 1$), a novel, generalized size parameter can be introduced that unifies the single scattering albedo (SSA) dependence on particle size parameter x independent of complex refractive index. In the large particle limit ($x >> 1$), SSA becomes independent of size parameter and decreases with increasing product of imaginary part of the refractive index and size parameter κx,

another generalized parameter, until $\kappa x \approx 1$, then stays fairly constant until κ becomes comparable with $n - 1$. Beyond this point, particles start to acquire metallic character and SSA quickly increases with κ and approaches one.

Acknowledgments

The work of HM has been supported by NASA EPSCoR under Cooperative Agreement No. NNX14AN24A, NASA ROSES under Grant No. NNX15AI48G, the National Science Foundation under Grant No. AGS-1544425, and the National Science Foundation's Solar Energy-Water-Environment Nexus in Nevada under Cooperative Support Agreement No. EPS- IIA-1301726. CMS has been supported by the National Science Foundation under Grants No. AGS-1261651 and AGS-1649783.

Data reported in the text and in the figures can be directly calculated by using the equations given here and in the relevant references. For Mie theory calculations, we used the IDL code mie_single.pro downloaded from http://eodg.atm.ox.ac.uk/MIE/mie_single.html.

References

[1] Acquista C, Cohen A, Cooney JA, Wimp J. Asymptotic behavior of the efficiencies in Mie scattering. J Opt Soc Am 1980;70(8):1023–5.
[2] Berg MJ, Sorensen CM, Chakrabarti A. A new explanation of the extinction paradox. J Quant Spectrosc Radiat Transfer 2011;112(7):1170–81.
[3] Bohren CF, Herman BM. Asymptotic scattering efficiency of a large sphere. J Opt Soc Am 1979;69(11):1615–16.
[4] Bohren CF, Huffman DR. Absorption and scattering of light by small particles, xiv. New York: Wiley; 1998. p. 530.
[5] Chýlek P. Asymptotic limits of the Mie-scattering characteristics. J Opt Soc Am 1975;65(11):1316–18.
[6] Chýlek P, Wong J. Effect of absorbing aerosol on global radiation budget. Geophys Res Lett 1995;22(8):929–31.
[7] Deirmendjian D. Electromagnetic scattering on spherical polydispersions, New York, NY: American Elsevier Publishing Company, Inc.; 1969. 318 pp.
[8] Hassan T, Moosmüller H, Chung CE. Coefficients of an analytical aerosol forcing equation determined with a Monte-Carlo radiation model. J Quant Spectrosc Radiat Transfer 2015;164:129–36.
[9] Heinson WR, Chakrabarti A, Sorensen CM. A new parameter to describe the transition of light scattering by an arbitrary sphere. Opt Commun 2015;356:612–15.
[10] Herman BM. Infra-red absorption, scattering, and total attenuation cross-sections for water spheres. Q J R Meteorol Soc 1962;88(376):143–50.
[11] Lorentz HA. Ueber die Beziehung zwischen der Fortpflanzungsgeschwindigkeit des Lichtes und der Körperdichte. Ann Physik 1880;245(4):641–65.
[12] Lorenz L. Ueber die refractionsconstante. Ann Physik 1880;247(9):70–103.
[13] Mie G. Beiträge zur Optik trüber Medien, speziell kolloidaler Metallösungen. Ann Physik 1908;330(3):377–445.
[14] Moosmüller H, Arnott WP. Angular truncation errors in integrating nephelometry. Rev Sci Instrum 2003;74(7):3492–501.
[15] Moosmüller H, Arnott WP. Particle optics in the Rayleigh regime. J Air Waste Manage Assoc 2009;59(9):1028–31.
[16] Moosmüller H, Chakrabarty RK, Arnott WP. Aerosol light absorption and its measurement: a review. J Quant Spectrosc Radiat Transfer 2009;110(11):844–78.
[17] Moosmüller H, Ogren JA. Parameterization of the aerosol upscatter fraction as function of the backscatter fraction and their relationships to the asymmetry parameter for radiative transfer calculations. Atmosphere 2017;8(133). doi:10.3390/atmos8080133.
[18] Piedra P, Moosmüller H. Optical losses of photovoltaic cells due to aerosol deposition: role of particle refractive index and size. Sol Energy 2017;155:637–46.
[19] Sorensen CM. Light scattering by fractal aggregates: a review. Aerosol Sci Tech 2001;35(2):648–87.
[20] van de Hulst HC. Light scattering by small particles, New York: Dover Publications; 1981. 470 pp.
[21] Wang G, Chakrabarti A, Sorensen CM. Effect of the imaginary part of the refractive index on light scattering by spheres. J Opt Soc Am A 2015;32(7):1231–1235.